



Drastic promoting the visible photoreactivity of layered carbon nitride by polymerization of dicyandiamide at high pressure

Jinshui Cheng^a, Zhao Hu^a, Kangle Lv^{a,*}, Xiaofeng Wu^a, Qin Li^a, Yuhan Li^b, Xiaofang Li^c, Jie Sun^a

^a Key Laboratory of Catalysis and Materials Science of the State Ethnic Affairs Commission & Ministry of Education, Hubei Province, College of Resources and Environmental Science, South-Central University for Nationalities Wuhan 430074, PR China

^b Engineering Research Center for Waste Oil Recovery Technology and Equipment, Ministry of Education, Chongqing Key Laboratory of Catalysis and New Environmental Materials, Chongqing Technology and Business University, Chongqing 400067, PR China

^c College of Chemistry and Chemical Engineering, Wuhan University of Science and Technology, Wuhan 430081, PR China



ARTICLE INFO

Keywords:

Carbon nitride
Dicyandiamide
Visible photoreactivity
Hydrogen production
High pressure

ABSTRACT

As a typical metal-free layered organic semiconductor photocatalyst, carbon nitride suffers from low light harvesting ability and unsatisfied photocatalytic activity ascribed to insufficient optical absorption and strongly bound exciton. In this paper, we reported the fabrication of a well crystallized carbon nitride with superior visible-light-driven photoreactivity by simply polymerization of dicyandiamide in a closed stainless steel autoclave which is used to afford a high pressure reaction environment. High pressure induced polymerization of dicyandiamide not only prevents the emission of hazardous gas, improving the yield of carbon nitride, but also enhances the crystallization of carbon nitride. The 550 °C calcined sample at high pressure (HP550) extends the interplanar packing distance of layered carbon nitride from 0.676 nm to 0.697 nm while compacts the layered-stacking distance from 0.327 nm to 0.322 nm when compared its counterpart that was synthesized under other identical conditions but at normal pressure (NP550). HP550 exhibits the highest photocatalytic activity towards hydrogen production ($772.40 \text{ umol}^{-1}\text{h}^{-1}\text{g}^{-1}$) under visible light irradiation ($\lambda \geq 420 \text{ nm}$), which is 7.8 times higher than that of NP550. The drastic improved photocatalytic activity of carbon nitride prepared at high pressure was attributed to the negatively shifted position of conductor band potentials, increased visible-light absorption and efficient separation of charge carriers, benefiting from the reduced $\pi-\pi$ layer stacking distance and breaking of intraplanar hydrogen bonds.

1. Introduction

Semiconductor photocatalysis has attracted much attention due to its potential applications in clean energy production [1], environmental remediation [2], and fine chemical synthesis [3,4]. However, many photocatalysts do not absorb in the visible light region (400–800 nm) that accounts for 43% of the incoming solar spectrum. Since Wang and co-workers first demonstrated carbon nitride as a promising visible-light photocatalyst for water splitting to produce hydrogen in 2009 [5], strenuous efforts have been devoted to synthesizing carbon nitride by thermal treatment of nitrogen-rich precursors such as urea [6], thiourea [7–9], melamine [10,11] and dicyandiamide [12,13]. As a metal-free layered material, carbon nitride is featured with graphitic π -conjugated structure, consisting of sp^2 hybridized tri-s-triazine repeating units in planes and weak covalence between layers [7]. Different from other common layered compounds, there are abundant hydrogen bonds in the covalent bonding dominated intralayer framework of carbon nitride

because of the incomplete polymerization of the precursors that contain amine groups. According to the study of Kang et al., the potential barriers between the layers and across the hydrogen bonds located regions are estimated to be 33.2 eV and 7.9 eV, respectively. The high barriers make the transport of photo-generated charge carriers between the layers and intralayer framework of carbon nitride very difficult [12], which result in the poor photocatalytic activity of layered carbon nitride. Therefore, how to stimulate the sluggish electrons of carbon nitride becomes a hot topic but still remains a great challenge [14].

Many efforts have been used to improve the photoreactivity of layered carbon nitride, which include nano-scaling technologies such as fabrication of nanosheet-like [15] or porous carbon nitride [12,13] by increasing the surface area and exposing the basal planes so as to increase the number of active site and reduce the diffusion distance for the transport of reactants and photo-generated acriers.

Doping or modification are usually used to improve the photocatalytic activity of carbon nitride. High photoreactivity of B [16] and C

* Corresponding author.

E-mail address: lvkangle@mail.scuec.edu.cn (K. Lv).

[17] doped carbon nitrides have been attributed to the increased visible light absorbance and electrical conductivity. To retard the recombination of photo-generated carriers, many works focused on coupling carbon nitride with carbon materials such as carbon dots [18] and graphene [19,20], with metals [21], with semiconductors such as TiO_2 [22–25], Ag_3PO_4 [26] and MOFs [27], and with photosensitizer such as porphyrin (CuTCPP) [28]. Our group found that the photoreactivity of carbon nitride is pH sensitive. Acidification of carbon nitride results in the formation of a localized surface state, which can act as a trapping site for photo-generated electrons [29]. It has also been proven that introduction of carbon [30] or nitrogen [31] vacancies into the lattice of carbon nitride by control the calcination atmosphere is another efficient-way to increase the photoreactivity of carbon nitride.

By post calcination of pristine carbon nitride powder in an argon atmosphere, Kang et al. prepared carbon nitride products with broken hydrogen bonds which easily form in the C–N covalent bonds-dominated intralayer framework of layered carbon nitride [12]. The enhanced photoreactivity was attributed to the increased band tails because of the destruction of intralayer long-range atomic order, and the formed abundant pores as a result of breaking of hydrogen bonds, which promotes the transfer of electrons to reach the lateral surface of the pores. Zhang et al. reported the synthesis of highly crystalline carbon nitride with an apparent quantum yield of as high as 57% of for H_2 evolution at 420 nm by co-condensation of urea and oxamide and followed by post-calcination in molten salt [6]. The high photoreactivity was attributed to the decreased optical band gap and improved lateral charge transport and interlayer exciton dissociation.

Recently, a novel strategy to promote the transfer of electrons was reported by Dong's group by intercalating alkalis into the interlayer space of carbon nitride so as to create a vertical channel between the layers for directional electron delivery [7–9].

Carbon nitride powder was mostly synthesized by direct calcination of the nitrogen-containing precursor at 500–600 °C in open reaction system such as in a crucible. During the heat-induced polymerization process, enormous hazardous gas such as amines will release from the furnace, which not only reduces the yield of carbon nitride because of the steady evaporation of organics with low polymerization degree, but also causes serious air pollution. We believe that synthesis of carbon nitride in a closed reactor such stainless steel autoclave is a good choice to solve the problems mentioned above. It is also proposed that the produced high pressure in the closed reactor is also good for the improvement of the crystallization of carbon nitride, which can reduce the defects and therefore enhance the photoreactivity of carbon nitride. Therefore, we compared the synthesis of carbon nitride by polymerization of dicyandiamide at normal pressure (in an open reactor shown in Scheme 1A) and high pressure (in a closed reactor shown in Scheme 1B) systems. Unexpectedly, the aims of both extending the visible-light-responsive range and promoting the transfer of photo-generated carriers were achieved by polymerization of dicyandiamide in high pressure system. The visible photoreactivity of layer carbon

nitride prepared at high pressure for water splitting to produce hydrogen drastically promoted 7.8 times when compared with that of the counterpart synthesized at normal pressure. Note that the closed reactor can be used for massive production of high photoreactive carbon nitride.

2. Experimental

2.1. Materials and synthesis

Dicyandiamide ($\text{C}_2\text{H}_4\text{N}_4$, 99%, Aladdin) was selected as precursor and used without further purification. High pressure carbon nitride was synthesized by thermal polycondensation of dicyandiamide in a closed reactor (Scheme 1B). Typically, a 10 mL alumina crucible with cover containing 3.0 g of dicyandiamide in a 50 mL closed stainless steel reactor was placed into the muffle furnace, which was then heated at 550 °C for 4 h with a heating rate of 5 °C min⁻¹ for thermal polycondensation. After cooling down to room temperature, the powder was collected and ground in a mortar. The obtained sample is denoted as HP550. Normal pressure carbon nitride sample was also prepared at 550 °C but using an open crucible as reactor (Scheme 1A), and the product is denoted as NP550.

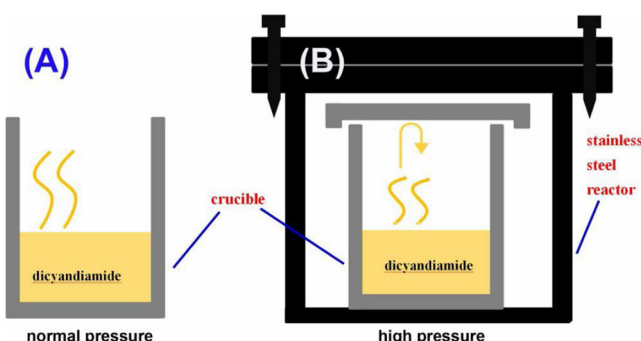
To systematically studied the effect of calcination temperature on the structure and performance of carbon nitride, polymerization of dicyandiamide experiments were performed at different temperatures (500–600 °C). The products prepared in open crucible (normal pressure) and in closed stainless steel reactor (high pressure) are denoted as NP x and HP x , respectively, where x represents the calcination temperature (Table 1).

2.2. Characterization

X-ray powder diffraction (XRD) data were collected on a D8-advance X-ray diffractometer (German Bruker) using $\text{Cu K}\alpha$ radiation at a scan rate of 0.02° 2 θ s⁻¹. The accelerated voltage and applied current were 15 kV and 20 mA, respectively. Using a field emission scanning electron microscopy (SEM) and a transmission electron microscopy (TEM) to observe the morphological characteristics and microstructures of the samples, the former was performed on an S-4800 Field Emission SEM (FESEM, Hitachi, Japan) at an accelerating voltage of 10 kV, while the latter was taken on a JEM-2100F electron microscope (JEOL, Japan) at 200 kV. FT-IR spectrum was recorded on a NEXUS-470 infrared spectrometer (Nicolet Co., U.S.A.). X-ray photoelectron spectroscopy (XPS) measurements were done with a Kratos XSAM800 XPS system with $\text{Mg K}\alpha$ source and a charge neutralizer, all the binding energies were referenced to the C 1 s peak at 284.8 eV of the surface adventitious carbon. The BET surface area was analyzed by N_2 adsorption in a nitrogen adsorption apparatus (Micromeritics ASAP 2020, USA), which was calculated from the adsorption data in the relative pressure (P/P_0) range of 0.05–0.3 via multipoint BET method. The catalyst was degassed at 200 °C for 4 h before N_2 adsorption measurements. UV-vis diffuse reflectance spectrum (DRS) was recorded on a UV-vis spectrophotometer (UV-2550, Shimadzu, Japan), and BaSO_4 was used as a reflectance standard. The photoluminescence (PL) spectrum was recorded on a Fluorescence Spectrophotometer (F-7000, Hitachi, Japan) at an excitation wavelength of 380 nm. PL decay spectrum was monitored at room temperature with a fluorescence spectrophotometer (Edinburgh Instruments, FLSP-920), and the excitation wavelength was set to 330 nm. Electron paramagnetic resonance (EPR) signal of the photocatalyst was recorded in an EPR spectrometer (JES-FA 200, JEOL) at room temperature (298 K) with a modulation frequency of 100 kHz and a microwave power of 0.99 mW.

2.3. Photoelectrochemical measurements

The electrochemical workstation (CHI760e, Shanghai, China) was



Scheme 1. Diagram of the reactors used for heat polymerization of dicyandiamide under normal pressure (A) and high pressure (B).

Table 1
Physical property of the photocatalyst.

Sample	Temperature ^a (°C)	Pressure ^b	Yield ^c (%)	S _{BET} (m ² g ⁻¹)	PV ^d (cm ³ g ⁻¹)	RC ^e	Bandgap (eV)	Sub-bandgap (eV)
NP500	500	N.P.	55.2	6.2	0.032	1.00	2.74	–
NP525	525	N.P.	49.5	10.5	0.052	0.98	2.74	–
NP550	550	N.P.	42.0	7.8	0.039	0.96	2.62	–
NP575	575	N.P.	35.2	13.9	0.079	1.11	2.66	–
NP600	600	N.P.	20.2	22.6	0.12	1.22	2.68	–
HP500	500	H.P.	73.7	4.0	0.018	–	2.84	–
HP525	525	H.P.	60.7	11.2	0.056	1.77	2.79	–
HP550	550	H.P.	51.8	6.2	0.027	2.24	2.77	2.09
HP575	575	H.P.	52.9	4.3	0.022	2.41	2.10	1.98
HP600	600	H.P.	47.2	7.4	0.032	2.44	2.76	2.01

^a calcination temperature during preparation of g-C₃N₄.

^b polymerization of dicyandiamide (C₂H₄N₄) at normal pressure (N.P.) or high pressure (H.P.).

^c yield of the product based on the weight ratio of g-C₃N₄ to dicyandiamide.

^d pore volume of the photocatalyst.

^e relative crystallinity of the photocatalyst calculated based on the (002) peak intensity of NP500 sample.

employed to measure transient photocurrent, EIS Nyquist plots and Mott-Schottky plots in a standard three-electrode system, using Pt wire as the counter electrode, the prepared samples and Ag/AgCl in saturated KCl as the working electrode and reference electrode, respectively. Na₂SO₄ aqueous solution (0.4 M) was used as electrolyte solution. The working electrode was prepared on a glassy carbon electrode in the Mott-Schottky measurement which was obtained under direct current potential polarization at a fixed frequency. Before the test of photocurrent, 50 mg photocatalysts and 30 μL Nafion were dispersed into 1 mL water/absolute ethanol mixed solvent(v/v = 1/1), and then the mixed aqueous solution was dispersed uniformly through ultrasound to form a homogeneous catalyst colloid. The ITO/carbon nitride electrode was prepared using the as-prepared carbon nitride colloid as precursor via drip coating method. A 3 W LED lamp emitted mainly at 420 nm was used as the light source (Shenzhen LAMPLIC, China).

2.4. Evaluation of the photocatalytic activity

The photocatalytic activity of the prepared carbon nitride sample was evaluated by hydrogen production from water splitting in a sealed three-necked bottle under N₂ protection. A 350 W Xenon arc lamp with an optical cut-off filter (420 nm) was used as a light source, and the light intensity for hydrogen production was measured to be 440 mW/cm². The distance is 20 cm between light source and reactor, and reaction temperature was kept at 25 ± 2 °C by using an external water circulation system. In a typical experiment, 50 mg of carbon nitride photocatalyst was added into the mixed solution of triethanolamine (TEA, 8 mL) and water (72 mL). Then 150 μL of H₂PtCl₆ solution (10 g L⁻¹) was dropwise added to the above solution to obtain 1.0 wt% Pt loaded carbon nitride photocatalyst by a photochemical reduction method under the irradiation of Xenon Arc lamp. The reactor is sealed after bubbled with nitrogen for 30 min to remove the dissolved oxygen. After illuminated for 1.0 hour under magnetic stir, 0.4 mL of gas was drawn out by a stainless steel syringe, and the concentration hydrogen in mixed gas was analyzed by a gas chromatograph (GC2018, Shimazu, Japan).

3. Results and discussion

3.1. Morphology and XRD

Fig. 1 compares the optical images of all the photocatalysts calcined at different temperature under normal (Fig. 1a–e) or high pressure (Fig. 1f–j). It can be seen that the color of HP500 is grey, which is much lighter than that of NP500 (pale yellow), indicating the poor polymerization of HP500 sample. However, when calcination temperature is higher than 525 °C, the color of HPx sample becomes much heavier

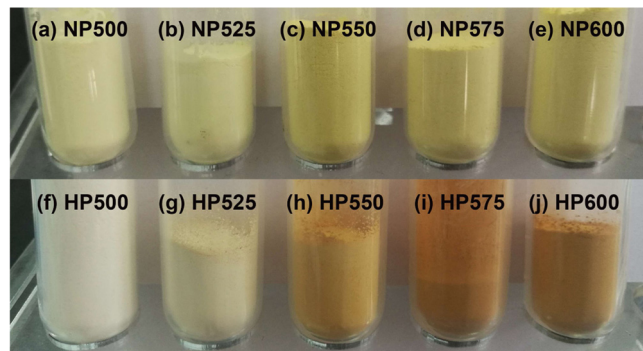


Fig. 1. Optical images of the photocatalysts prepared by heat polymerization of dicyandiamide (C₂H₄N₄) under normal pressure (a–e) and high pressure (f–j).

than that of NPx sample. For example, HP550 sample is brown, while NP550 is light yellow. From the different color of the product, we can predict that high pressure facilitates the crystallization of carbon nitride, which will be proven by the XRD characterization results.

From Table 1, we can see that the yield of layered carbon nitride obtained from high pressure system increases 10%–30% when compared with that in normal pressure system at the same calcination temperature, indicating that this method can not only increase the product, but also reduce the emission of hazardous gas.

Fig. 2A and B depicts the XRD patterns of NPx and HPx samples, respectively. It can be seen that all the samples (except HP500) showed two distinct peaks, albeit with different peak location and intensity. Two identical peaks located at 13.0° and 27.3°, corresponding to (100) interplanar packing of heptazine units and (002) π–π interlayer stacking motif, were recorded, indicating the successful fabrication of layered carbon nitride [6,32,33]. However, some impure peaks, except the (100) and (002) diffraction peaks for carbon nitride, were observed for HP500 sample (Fig. 2B), reflecting the incomplete polymerization of dicyandiamide at this stage [5].

When compared with that of NPx sample, the (002) diffraction peak of HPx sample (except HP500) is much narrower while the (100) diffraction peak is too weak to be observed. This indicates that high pressure facilitates the periodic stacking of layers of conjugated aromatic systems of carbon nitride but destroy the intralayer structural packing motif of tri-s-triazine units. Whatever at normal or high pressure, the (002) peak intensity of carbon nitride sample slightly increases with increasing the calcination temperature, indicating that high temperature favors for the polymerization reaction (Table 1). Therefore, both high pressure and high calcination temperature can enhance the crystallization of carbon nitride. Well crystallization means few defects,

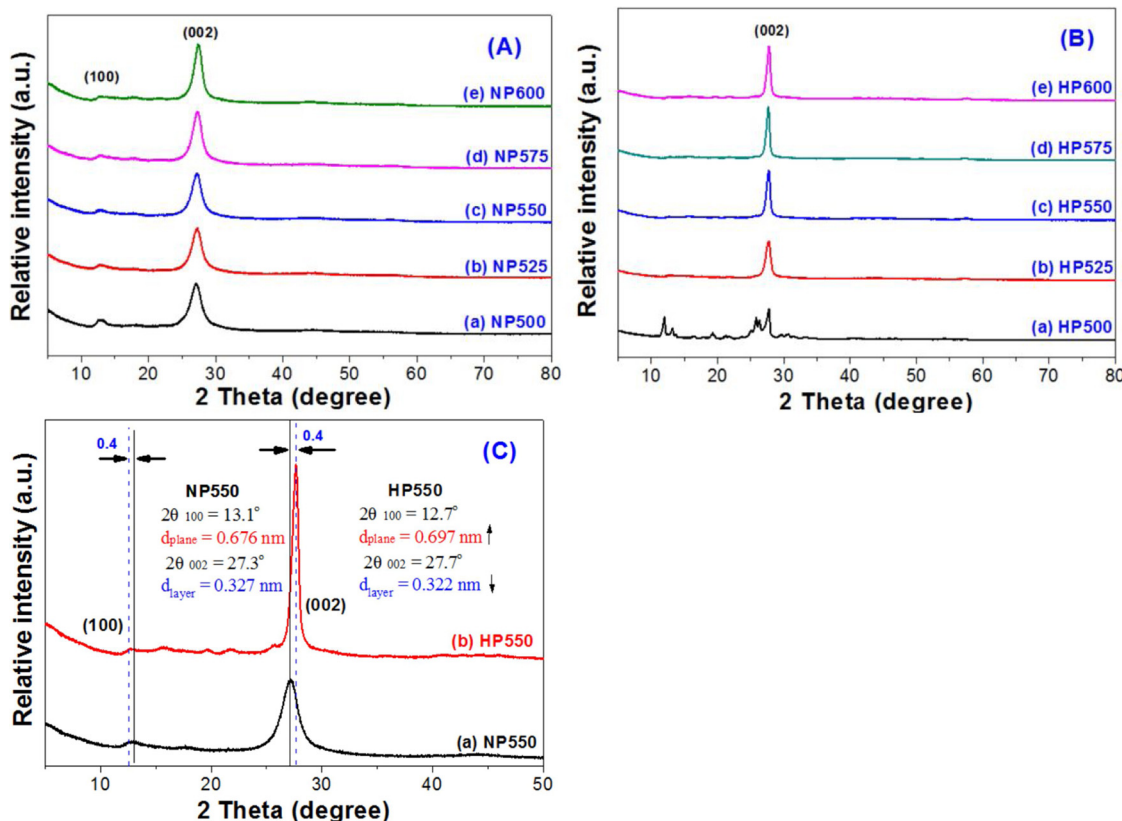


Fig. 2. XRD patterns of the photoatalysts calcined at different temperature in normal pressure (A) and high pressure (B), and the comparison of the XRD patterns between NP550 and HP550 samples (C).

which is beneficial to the photocatalytic activity of carbon nitride.

Fig. 2C further compares the XRD patterns of NP550 and HP550 samples. We can clearly see that the (100) peak intensity of HP550 is weaker than that of NP550, indicating that high pressure induces the breaking of the hydrogen bonds in the interplanar-framework of layered carbon nitride [12]. However, the (002) peak intensity of HP550 becomes much stronger. Carefully view shows that the (100) diffraction peak of HP550 shifts down from 13.1° to 12.7°, revealing an extended interplanar packing distance of about 0.697 nm for HP550 when compared with 0.676 nm for pristine carbon nitride (NP550), further confirmed that high pressure can break the hydrogen bonds between neighbouring melon strands [12].

In contrast, the (002) diffraction peak of HP550 sample shifts up from 27.3° to 27.7°, reflecting the fact that the interlayer stacking distance was compacted because of a strong van der Waals attraction between the neighboring heptazine layers. The stacking distances between neighbouring layers decreases from 0.327 nm (NP550) to 0.322 nm (HP550). It has been theoretically predicted that the layer stacking distance of layered carbon nitride dominates the interlayer exciton dissociation and thus charge mobility. Reducing the $\pi-\pi^*$ layer stacking distance of between layers can improve the lateral charge transport and interlayer exciton dissociation [6], enhancing the photocatalytic activity.

The well crystallization of HPx samples was also confirmed from their TEM images. When compare with the coarse surface of NP550 sample (Fig. 3f), the surfaces of HPx samples (Fig. 3a–e) are very smooth, indicating the reduction of surface defects. From the SEM images shown in Fig. 4, it can be seen that the texture of HP550 sample is more condense than that of NP550 due to the enhanced crystallization at high pressure (Fig. 2C).

3.2. FTIR and UV-vis absorption spectrum analysis

We further use the FTIR spectroscopy to compare the microstructures of the layered carbon nitride (Fig. S1). It can be observed that all samples (except HP500) exhibit obvious absorption peaks between 1900 and 700 cm⁻¹, which are typical bands of carbon nitride for the trigonal N(C)₃/bridging HN(C₂) units and heptazine ring of the melon unit in the strands [15,34]. When compared with NP550 sample, HP550 sample shows improved FTIR spectrum absorption (Fig. 5), further confirms the high pressure induced enhancement of crystallization, which is consistent with the XRD characterization results. This also indicates that high pressure only stretches the periodic arrangement of the melon strands within the layers (Fig. 2C), however the basic atomic structures of the strands keeps unchanged [12].

Light harvesting ability is of great importance to the photoreactivity of the photocatalyst. Therefore, we compared the UV-vis optical absorption spectra of the layered carbon nitride prepared at normal (Fig. 6A) and high pressure (Fig. 6B). It can be clearly seen that, when calcination temperature is higher than 550 °C, HPx samples show an obviously enhanced optical absorption whatever in UV or in visible light regions. The improved absorptive ability of HPx sample in UV region reflects the reinforced $\pi-\pi^*$ electron transition in the conjugated aromatic ring system to the tighter and better packing of the joint heptazine system due to the high pressure induced well crystallization.

Fig. 6C compares the diffuse reflectance spectra of NP550 and HP550 samples. Although the intrinsic absorption band of layered carbon nitride, originating from the $\pi-\pi^*$ electron transition of the sp² hybridization of C and N in the CN framework, blue-shifts from 466 nm (NP550) to 448 nm (HP550), an obvious new absorption band with an onset beginning at 692 nm is observed. This new band is usually ascribed to the n- π^* electron transition from the lone pairs of the edge nitrogen atoms in the heptazine units [6]. High pressure breaks the hydrogen bonds between neighbouring melon strands by extending the

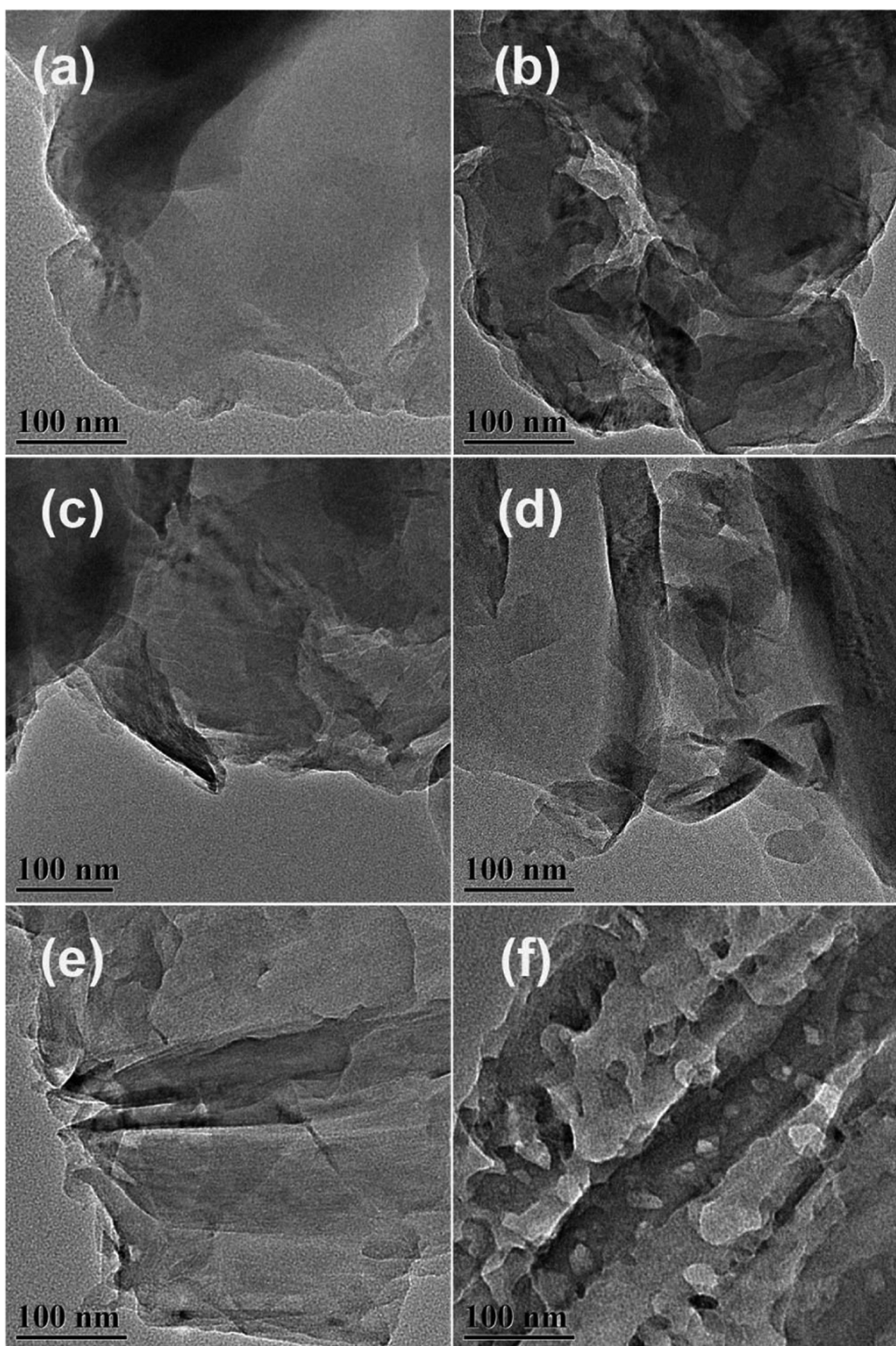


Fig. 3. TEM images of HP500 (a), HP525 (b), HP550 (c), HP575 (d), HP600 (e) and NP550 (f) samples, respectively.

interplanar packing distance (Fig. 2C), which therefore results in the $n-\pi^*$ electron transition due to the exposure of free edge nitrogen atoms on the sacrifice of hydrogen bonds.

Usually this $n-\pi^*$ electron transition is forbidden for perfectly symmetric and planar units, however, in the present study, high

pressure induced charged/polarized planar units and compacted interlayer stacking, allows access to this electron transition. The creation of new absorption band sharply improve the light responsive range of layered carbon nitride (Fig. 6).

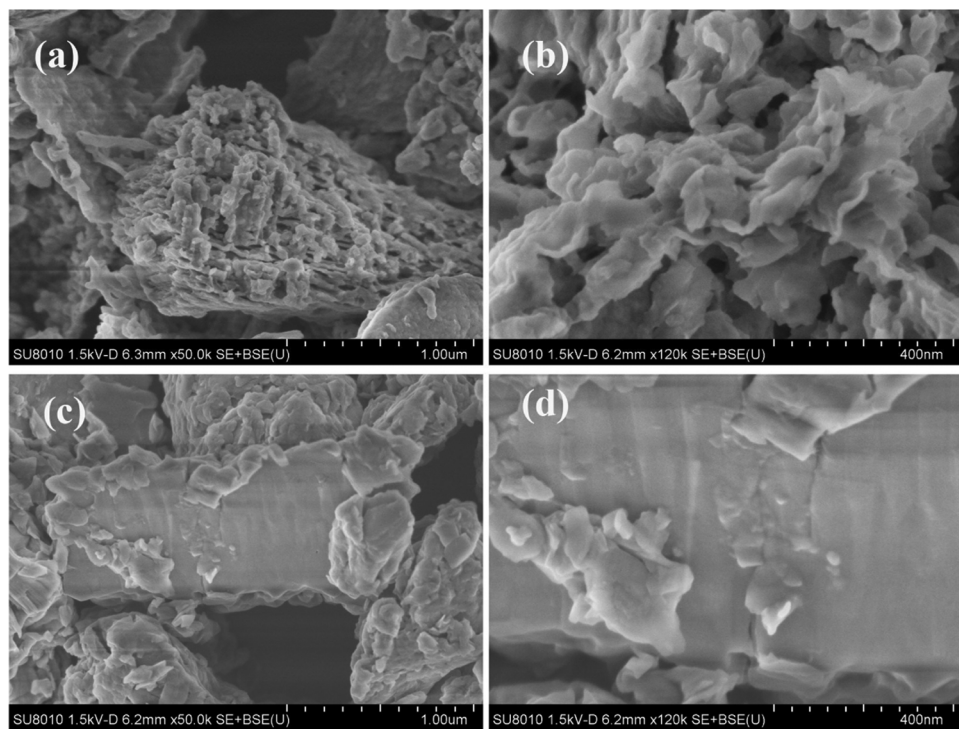


Fig. 4. SEM images of NP550 (a and b) and HP550 (c and d) samples.

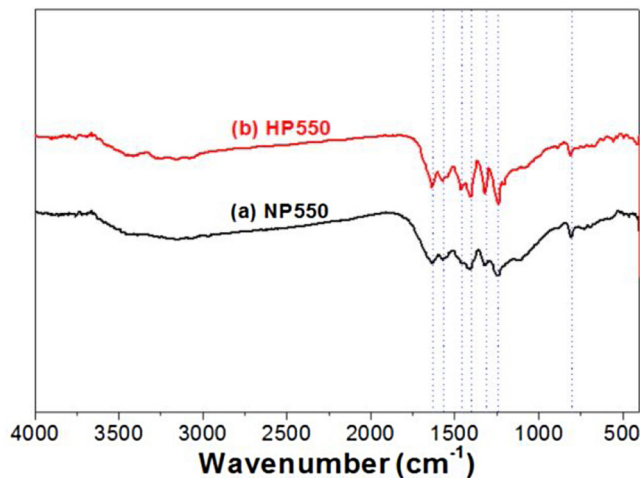


Fig. 5. Comparison of the FTIR spectra between NP550 and HP550 samples.

3.3. Nitrogen adsorption isotherms

The BET surface area is important factor influencing the photoreactivity. Therefore, we measured the nitrogen adsorption isotherms of the photocatalysts. Fig. 7 compares the nitrogen adsorption-desorption isotherms and the corresponding pore size distribution curves between NP550 and HP550 samples. It can be seen that both isotherms are type IV with hysteresis loops of type H3 at a relative pressure range of 0.5–1.0, suggesting narrow slit-shaped pores that are generally associated with plate-like particles [35], which agrees well with their layered structures (Fig. 3). The BET surface area of HP550 sample is $6.2 \text{ m}^2 \text{ g}^{-1}$, a little smaller than that of NP550 sample ($7.8 \text{ m}^2 \text{ g}^{-1}$). The smaller BET surface area of HP550 sample is due to the improved crystallization when compared with NP550 sample (Fig. 2C).

Table 1 lists the BET surface areas and pore volumes of the photocatalysts. It can be seen that HPx sample possesses both smaller BET surface area and pore volume than NPx sample calcined at the same

temperature due to the high pressure induced enhancement crystallization of HPx sample (Fig. 2).

3.4. Visible photocatalytic activity

The photocatalytic activity of the layered carbon nitride was evaluated by splitting water to produce hydrogen under visible light irradiation ($\lambda > 420 \text{ nm}$). From Fig. 8A, it can be seen that the photoreactivity of NPx steady increases with increase in the calcination temperature from 500°C to 600°C . This is because that high temperature induces polymerization of dicyandiamide[36]. The photoreactivity of HPx increases first and then decreases with an optimal calcination temperature of 550°C . Except HP500 sample, all the HPx samples possess obvious improved hydrogen production rate (HPR) than corresponding NPx samples. For example, the HPR of HP550 sample is as high as $772.40 \text{ umol h}^{-1} \text{ g}^{-1}$, which is 7.81 times higher than that of NP550 sample (only $98.96 \text{ umol h}^{-1} \text{ g}^{-1}$). The apparent quantum yield (AQY) of HP550 sample at 420 nm is 1.60% (see supporting information), which is two times higher than that of NP550 sample (only 0.75%).

On considering that the BET surface area can affect the evaluation of the photoreactivity, we compares the photocatalytic activity based on surface area-normalized HPR between NPx and HPx samples (Fig. 8B). The higher photocatalytic activity of HPx was further confirmed. Surface area-normalized HPR of HP550 ($124.58 \text{ umol h}^{-1} \text{ m}^{-2}$) is 9.82 times higher than that of NP550 ($12.69 \text{ umol h}^{-1} \text{ m}^{-2}$). This infers that the higher photoreactivity of carbon nitride prepared at high temperature is caused by other factors instead of the BET surface area.

3.5. X-ray photoelectron spectroscopy analysis

The chemical states of layered carbon nitride for NP550 and HP550 samples were investigated by X-ray photoelectron spectroscopy (XPS). Fig. S2A compares the XPS survey spectra of the two samples. It can be seen that both samples contain C and N with small amount of O elements, and the corresponding photoelectron peaks appears at binding energies of 288 (C 1s), 399 (N 1s), 532 eV (O 1s), respectively.

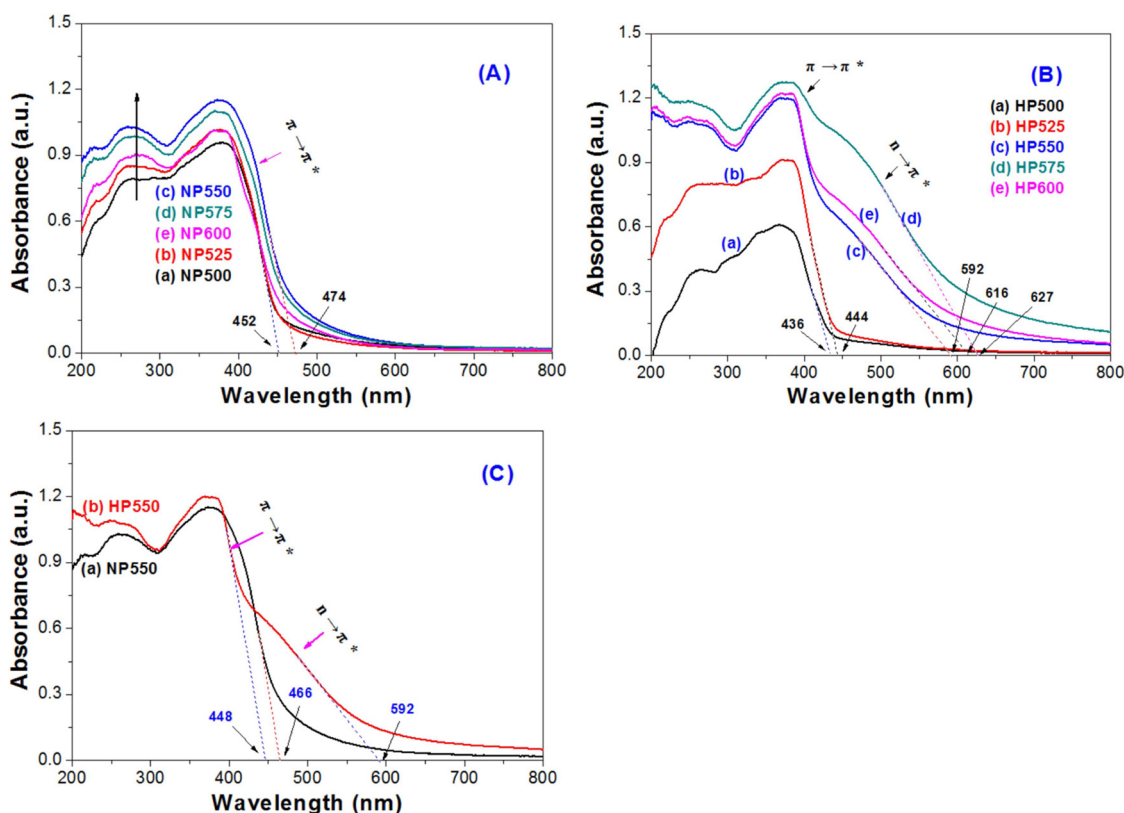


Fig. 6. Optical absorption spectra of the photocatalysts prepared in normal pressure (A) and high pressure (B), and the comparison of the absorption spectra between NP550 and HP550 samples (C).

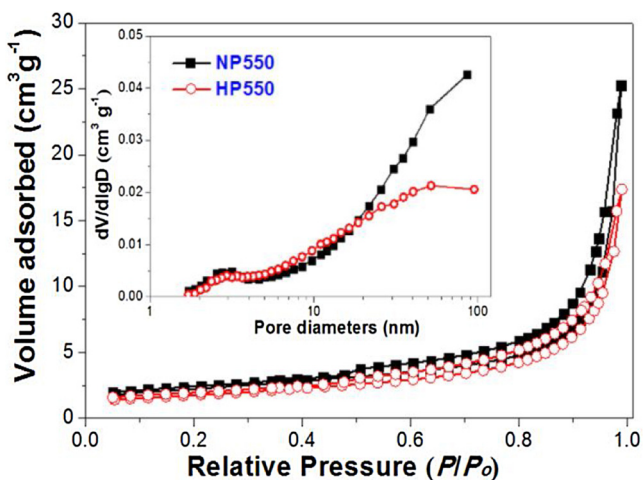


Fig. 7. Nitrogen sorption-desorption isotherms and the corresponding pore size distribution curves of NP550 and HP550 samples.

The high resolution XPS spectrum of C 1s peak can be deconvoluted into a smaller peak centered at 284.6 eV originating from the adventitious hydrocarbon from XPS instrument itself, and a larger peak centered at 287.7 eV corresponding to the three-coordinated carbon of N—C=N in the melon (Fig. S2B). The deconvolution of the overlapped N 1s peaks has produced three peaks centered at 398.3, 399.7 and 400.8 eV (Fig. S2C), which are associated with pyridine N, pyrrolic N, and graphitic N, respectively [23,37].

3.6. Photoluminescence spectrum and (photo)electrochemical property

To account for the superior photocatalytic activity of layered carbon

nitride prepared at high pressure, we monitored the steady state photoluminescence (PL) spectra of NPx and HPx samples. From Fig. S3, we can see that the PL intensity decreases with increase in the calcination temperature for both sets of carbon nitride samples, and the PL intensity for HPx sample (except HP500) is weaker than that of the corresponding NPx sample. This indicates that polymerization of di-cyandiamide at high temperature and high pressure leads to substantial suppression of radiative electron-hole recombination in carbon nitrides due to the improved crystallization induced reduction of surface defects (Fig. 2).

The PL spectrum of NP550 sample shows a strong emission peak at 469 nm, which is ascribed to the band-to-band recombination of carriers [29]. The band-to-band emission peak of HP550 sample blue-shifts to 452 nm (Fig. 9), consistent with its optical absorption spectrum (Fig. 6C).

Fig. 9B compares the time-resolved PL spectra between NP550 and HP550 sample, which clearly shows a quicker recombination of HP550. The average PL lifetime decreases from 20.52 ns for NP550 sample to 10.32 ns for HP550 sample (for lifetime components see Table S2). Because only the very fast charge pairs can recombine, the shorter singlet exciton lifetime of HP550 sample implies its enhanced exciton dissociation [6]. This is possibly due to the high pressure-induced well crystallization of HP550, which possesses shorter layer distance (Fig. 2C), beneficial to the charge transfer over the layers and dissociation of the singlet excitons. The improved charge transport of HP550 sample is also confirmed by the increased photocurrent (Fig. 10A) and decreased hemicycle radius measured by electrochemical impedance spectroscopy (Fig. 10B). According to the study of Liu et al. [12], the remarkable shortening of the PL lifetime and related suppression of the radiative recombination can also caused by the emergence of the band-tails-involved rapid radiative electron-hole recombination processes in carbon nitride with broken hydrogen bonds. An increased density of the band tails can act as shallow trap states of

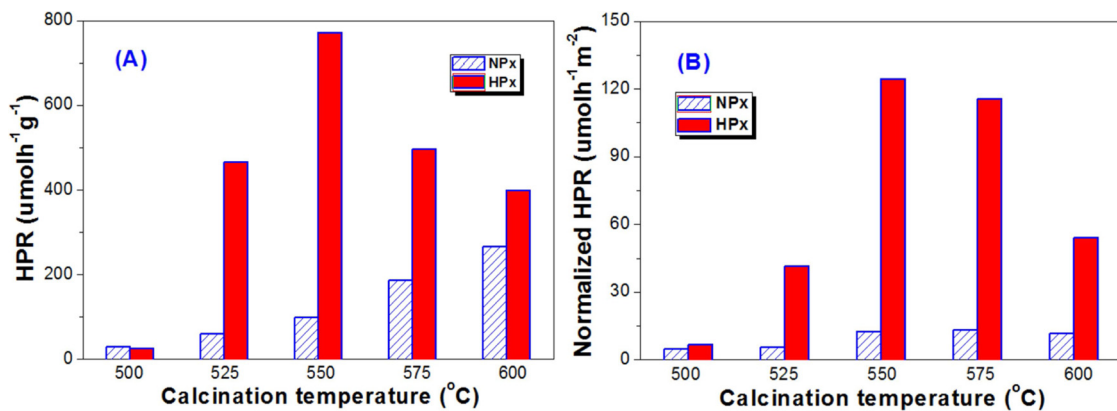


Fig. 8. Comparison of the apparent hydrogen production rate (A) and corresponding specific hydrogen production rate in unit of surface area of the photocatalyst (B) under visible light irradiation.

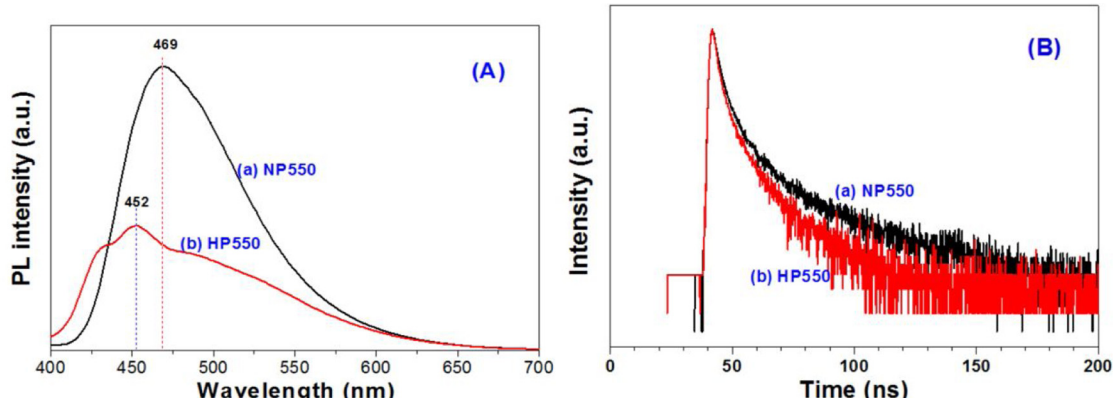


Fig. 9. Comparison of the photoluminescence spectra (A) and transient photoluminescence spectra (B) between NP550 and HP550 samples.

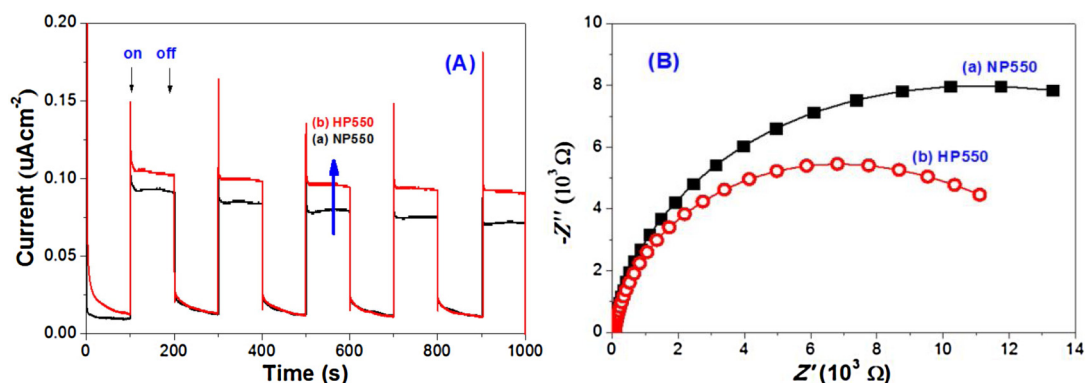


Fig. 10. Comparison of the photocurrent (A) and electrochemical impedance spectroscopy (B) between NP550 and HP550 samples.

photogenerated charge carriers, by breaking hydrogen bonds can enhance the probability of occurring of such rapid PL processes.

Electron paramagnetic resonance (EPR) measurements at room temperature show that HP550 sample has a greater ability to delocalize electrons when compared with NP550 sample (Fig. 11). As compared in Fig. 11A, both samples exhibit one single Lorentzian line with a g value of 2.001, which originates from the unpaired electrons in sp^2 -carbon in the aromatic rings [37]. The stronger EPR signal of HP550 sample can be explained by the reduced stacking distance between neighboring layers (Fig. 2C), which reveals that the electrons of π bonds can be extended to deviate from the basal planes and therefore the electron mobility within adjacent layers can be enormously boosted. Under the visible light irradiation, the intensity of EPR signal of the photocatalyst increases, indicating that these unpaired electrons in sp^2 -carbon in the

aromatic rings are responsible for the photogeneration of active radicals which can be used for photocatalytic reaction.

3.7. Electronic band structures

We further determined the electronic band structure of NP550 and HP550 samples by examining of Mott-Schottky plots. As can be seen from Fig. 12, both samples exhibit positive slopes in the Mott-Schottky plots at frequencies of 1.5, 2.5 and 3.0 kHz, and the flat band potentials of HP550 and NP550 determined based on the x-intercept in the Mott-Schottky plots are calculated to be -1.50 and -1.20 V (vs. Ag/AgCl), or -1.77 and -1.47 V (vs. NHE), respectively. By a combined analysis of bandgaps derived from the DRS spectra (Fig. 6C), the VB potentials of HP550 and NP550 are determined to be $+1.00$ and $+1.15$ V (vs. NHE),

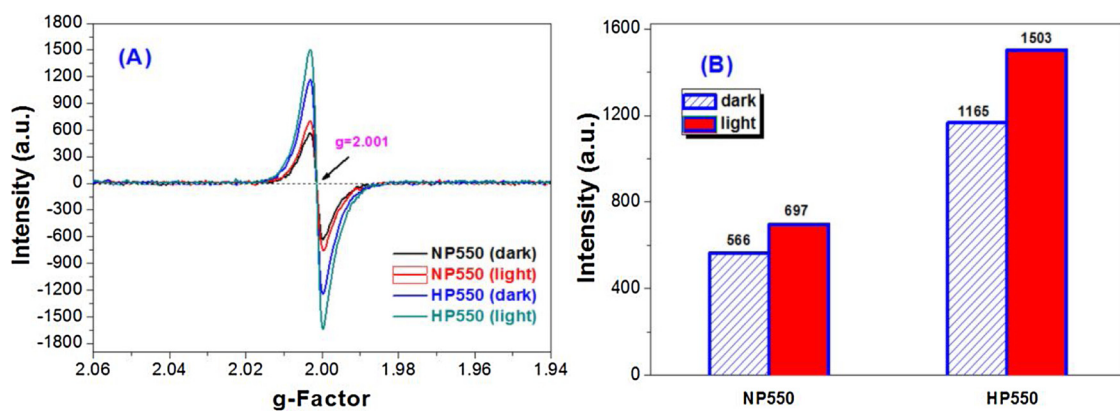


Fig. 11. EPR spectra (A) and comparison of the magnetic signal intensity (B) for NP550 and HP550 samples.

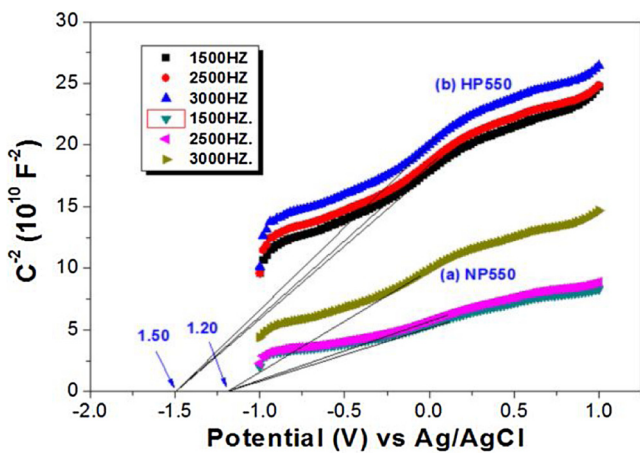


Fig. 12. Mott-Schottky plots of the photocatalysts measured in 0.4 M Na_2SO_4 aqueous solution.

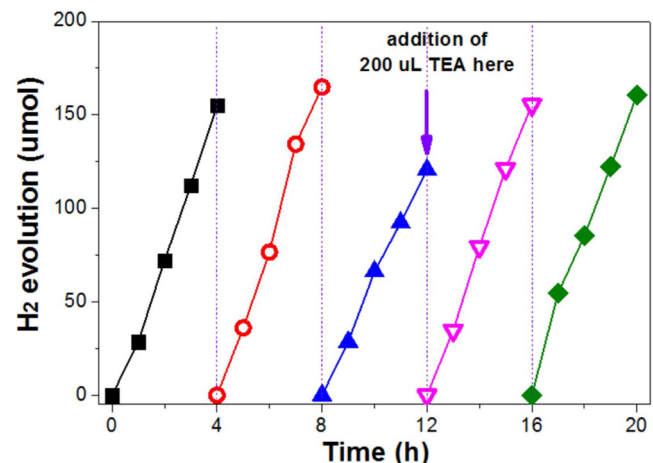
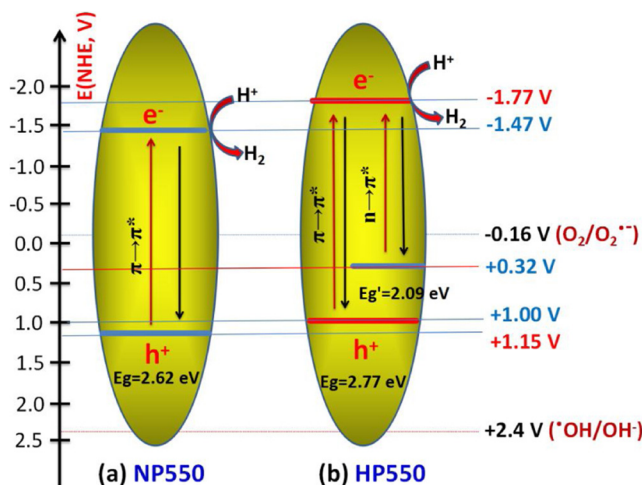


Fig. 13. Recycling use of HP550 photocatalyst for hydrogen production under visible irradiation.



Scheme 2. Comparison of the band structures between NP550 and HP550 samples.

respectively. These positions thermodynamically enable the reduction of proton for hydrogen production [13].

Scheme 2 compares the electronic band structures of HP550 and NP550 samples. It can be seen that high pressure induces negatively-shifted CB position of layered carbon nitride (HP550), which favors for the efficient capture of photo-generated electrons, sharply increasing the hydrogen production rate (Fig. 8). Although the intrinsic band gap of HP550 (2.77 eV) is larger than that of NP550 (2.62 eV), the broken

hydrogen bonds results in the formation of a sub-bandgap ascribed to the $n-\pi^*$ electron transition involving the lone pairs of the edge nitrogen atoms in the heptazine units. This new band sharply extends the visible-light-responsive range of layered carbon nitride, which makes it can use solar energy for photochemistry.

Note that the high photoreactive HP550 sample shows very stable photocatalytic activity, which shows little decrease in HPR even after 4 successive runs under visible light irradiation (Fig. 13). So the reported layered carbon nitride prepared at high pressure has the merits of high yield, high photocatalytic activity and high stability.

4. Conclusions

High photoreactive layered carbon nitride with greatly extended visible-light-responsive range was successfully fabricated by simply polymerization of dicyandiamide in a closed stainless steel autoclave which affords a high pressure reaction environment. Polymerization of dicyandiamide in this closed autoclave can not only prevent the emission of hazardous gas, improving the yield of carbon nitride, but also enhance the crystallization of carbon nitride, boosting the visible photocatalytic activity. The ultrahigh solar hydrogen production activity of the layered carbon nitride prepared in this close autoclave is attributed to the compacted layered-stacking distance which is beneficial to the charge transfer over the layers, and the breaking of hydrogen bonds existing in the C–N covalent bonds-dominated intralayer framework which therefore broaden the light-responsive range of carbon nitride by facilitating the $n-\pi^*$ electron transition involving the lone pairs of the edge nitrogen atoms in the heptazine units. The present

study provided new insights into the mechanistic understanding and the design of electronically optimized layered photocatalysts for enhanced solar energy conversion.

Acknowledgments

This work was supported by the National Natural Science Foundation of China (51672312 & 21373275), the Science and Technology Program of Wuhan (2016010101010018) and the Fundamental Research Funds for the Central University, South-Central University for Nationalities (CZT18016).

Appendix A. Supplementary data

Supplementary material related to this article can be found, in the online version, at doi:<https://doi.org/10.1016/j.apcatb.2018.03.066>.

References

- [1] Q.J. Xiang, B. Cheng, J.G. Yu, *Angew. Chem. Int. Ed.* 54 (2015) 11350–11366.
- [2] J.X. Low, J.G. Yu, W.K. Ho, *J. Phys. Chem. Lett.* 6 (2015) 4244–4251.
- [3] F.Z. Su, S.C. Mathew, G. Lipner, X.Z. Fu, M. Antonietti, S. Blechert, X.C. Wang, *J. Am. Chem. Soc.* 132 (2010) 16299–16301.
- [4] R.W. Yang, J.H. Cai, K.L. Lv, X.F. Wu, W.G. Wang, Z.H. Xu, M. Li, Q. Li, W.Q. Xu, *Appl. Catal. B* 210 (2017) 184–193.
- [5] X.C. Wang, K. Maeda, A. Thomas, K. Takanabe, G. Xin, J.M. Carlsson, K. Domen, M. Antonietti, *Nat. Mater.* 8 (2009) 76–80.
- [6] G.G. Zhang, G.S. Li, Z.A. Lan, L.H. Lin, A. Savateev, T. Heil, S. Zafeiratos, X.C. Wang, M. Antonietti, *Angew. Chem. Int. Ed.* 56 (2017) 13445–13449.
- [7] J.Y. Li, W. Cui, Y.J. Sun, Y.H. Chu, W.L. Cen, F. Dong, *J. Mater. Chem. A* 5 (2017) 9358–9364.
- [8] T. Xiong, W.L. Cen, Y.X. Zhang, F. Dong, *ACS Catal.* 6 (2016) 2462–2472.
- [9] W. Cui, J.Y. Li, W.L. Cen, Y.J. Sun, S.C. Lee, F. Dong, *J. Catal.* 352 (2017) 351–360.
- [10] H.H. Ou, P.J. Yang, L.H. Lin, M. Anpo, X.C. Wang, *Angew. Chem. Int. Ed.* 56 (2017) 10905–10910.
- [11] C.L. Wang, L.M. Hu, B. Chai, J.T. Yan, J.F. Li, *Appl. Surf. Sci.* 430 (2018) 243–252.
- [12] Y.Y. Kang, Y.Q. Yang, L.C. Yin, X.D. Kang, L.Z. Wang, G. Liu, H.M. Cheng, *Adv. Mater.* 28 (2016) 6471–6477.
- [13] Q.H. Liang, Z. Li, Z.H. Huang, F.Y. Kang, Q.H. Yang, *Adv. Funct. Mater.* 25 (2015) 6885–6892.
- [14] S.W. Cao, J.G. Yu, *J. Phys. Chem. Lett.* 5 (2014) 2101–2107.
- [15] P. Niu, L.L. Zhang, G. Liu, H.M. Cheng, *Adv. Funct. Mater.* 22 (2012) 4763–4770.
- [16] S.C. Yan, Z.S. Li, Z.G. Zou, *Langmuir* 26 (2010) 3894–3901.
- [17] G.H. Dong, K. Zhao, L.Z. Zhang, *Chem. Commun.* 48 (2012) 6178–6180.
- [18] S. Fang, Y. Xia, K.L. Lv, Q. Li, J. Sun, M. Li, *Appl. Catal. B* 185 (2016) 225–232.
- [19] G.Z. Liao, S. Chen, X. Quan, H.T. Yu, H.M. Zhao, *J. Mater. Chem.* 22 (2012) 2721–2726.
- [20] J.P. Zou, L.C. Wang, J.M. Luo, Y.C. Nie, Q.J. Xing, X.B. Luo, H.M. Du, S.L. Luo, S.L. Sui, *Appl. Catal. B* 193 (2016) 103–109.
- [21] Y.H. Li, K.L. Lv, W.K. Ho, Z.W. Zhao, H. Yu, *Chin. J. Catal.* 38 (2017) 321–329.
- [22] Y.H. Li, K.L. Lv, W.K. Ho, F. Dong, X.F. Wu, Y. Xia, *Appl. Catal. B* 202 (2017) 611–619.
- [23] Z.A. Huang, Q. Sun, K.L. Lv, Z.H. Zhang, M. Li, B. Li, *Appl. Catal. B* 164 (2015) 420–427.
- [24] Y.C. Nie, F. Yu, L.C. Wang, Q.J. Xing, X. Liu, Y. Pei, J.P. Zou, W.L. Dai, Y. Li, S.L. Suib, *Appl. Catal. B* 227 (2018) 312–321.
- [25] X.H. Jiang, Q.J. Xing, X.B. Luo, F. Li, J.P. Zou, S.S. Liu, X. Li, X.K. Wang, *Appl. Catal. B* 228 (2018) 29–38.
- [26] Y.M. He, L.H. Zhang, B.T. Teng, M.H. Fan, *Environ. Sci. Technol.* 49 (2015) 649–656.
- [27] G. Zhou, M.F. Wu, Q.J. Xing, F. Li, H. Liu, X.B. Luo, J.P. Zou, J.M. Luo, A.Q. Zhang, *Appl. Catal. B* 220 (2018) 607–614.
- [28] D.M. Chen, K.W. Wang, W.Z. Hong, R.L. Zong, W.Q. Yao, Y.F. Zhu, *Appl. Catal. B* 166–167 (2015) 366–373.
- [29] S. Fang, K.L. Lv, Q. Li, H.P. Ye, D.Y. Du, M. Li, *Appl. Surf. Sci.* 358 (2015) 336–342.
- [30] Y.H. Li, W.K. Ho, K.L. Lv, B.C. Zhu, S.C. Lee, *Appl. Surf. Sci.* 430 (2018) 380–389.
- [31] G.H. Dong, W.K. Ho, C.Y. Wang, *J. Mater. Chem. A* 3 (2015) 23435–23441.
- [32] F. Dong, L.W. Wu, Y.J. Sun, M. Fu, Z.B. Wu, S.C. Lee, *J. Mater. Chem.* 21 (2011) 15171–15174.
- [33] T. Sano, S. Tsutsui, K. Koike, T. Hirakawa, Y. Teramoto, N. Negishi, Koji Takeuchi, *J. Mater. Chem. A* 1 (2013) 6489–6496.
- [34] F. Dong, Z.Y. Wang, Y.H. Li, W.K. Ho, S.C. Lee, *Environ. Sci. Technol.* 48 (2014) 10345–10353.
- [35] Z.Y. Wang, K.L. Lv, G.H. Wang, K.J. Deng, D.G. Tang, *Appl. Catal. B* 100 (2010) 378–385.
- [36] W.J. Ong, L.L. Tan, Y.H. Ng, S.T. Yong, S.P. Chai, *Chem. Rev.* 116 (2016) 7159–7329.
- [37] S.N. Li, G.H. Dong, R. Hailili, L.P. Yang, Y.X. Li, F. Wang, Y.B. Zeng, C.Y. Wang, *Appl. Catal. B* 190 (2016) 26–35.